Available online at www.sciencedirect.com
SCIENCE DIRECT®
International Journal of Thermal Sciences 45 (2006) 209–216
International Journal of Thermal Sciences
www.elsevier.com/locate/ijts

Heat transfer and nucleation in pool-boiling

Erich Hahne *, Gerrit Barthau

Universität Stuttgart, Institut für Thermodynamik und Wärmetechnik, Pfaffenwaldring 6, 70550 Stuttgart, Germany

Received 8 March 2004; received in revised form 19 October 2004; accepted 19 October 2004

Available online 25 October 2005

Abstract

The creation of bubbles is a fundamental process in boiling heat transfer. There must be a correlation between heat transfer and bubble action. In order to find out more about it a number of tubes of different materials, diameters and surface finish were investigated and their heat transfer coefficients were determined. Besides the overall heat transfer coefficient, local heat transfer coefficients on the circumference of a stainless steel tube were obtained. A comparison of measurements made in Stuttgart with those made in Paderborn (one of our partners in a joint program financed by the Deutsche Forschungsgemeinschaft) showed very good agreement.

In order to count nucleation sites and determine nucleation site densities, observations were made over periods of 15 to 30 minutes (long term observations) and for periods of 1/60 second (short term observations). The results were called accordingly long term- or short term nucleation site densities.

Results for either observation time are given in diagrams. Clear differences appear for different tube materials, different surface finish and long—or short term observations.

Emery ground Cu-tubes show distinctly a different nucleation behaviour from gold-plated, sandblasted Cu-tubes.

The heat flow from a single active site was determined and it was tried to correlate this with the average bubble spacing. So far, such a correlation is best acceptable for spacings larger than 1 mm, i.e. for only a very small nucleation site density.

Keywords: Nucleate pool boiling; Nucleation site density; Critical radius; Average bubble spacing; Average bubble heat flow; Heating wall properties; R134a

1. Introduction

Observation of boiling phenomena shows bubbles emerging irregularly from single spots on a heated surface. A microscopic survey of such surfaces reveals tiny scratches or cavities in the material where bubbles are formed. These cavities are called nuclei, the whole process nucleation and the regime nucleate boiling or nucleation.

Clearly the number of such nuclei sites must be an important parameter in nucleate boiling. Investigations have been performed since many years. Jakob and Fritz [1] and Jakob and Linke [2] counted already in 1931 visually the number of active nucleation sites and measured heat transfer coefficients.

In later years a number of investigations have been performed to count active (bubble producing) sites, both by direct observation and by still or high speed photography [1–22].

These counts were restricted to small site numbers per area (= nucleation site density) $N/A < 100\ \mathrm{cm}^{-2}$ and consequently to low heat fluxes. At high heat fluxes with larger N/A a great number of bubbles float in the liquid and obscure the view on the heated surface.

New methods have been developed to overcome this problem.

Gaertner and Westwater [23] studied nucleate boiling on an electroplated surface and identified up to 175 sites·cm^{-2}.

Semeria [24] observed more than 1000 bubble-columns·cm^{-2} on a thin wire.

Kirby and Westwater [25] found up to 630 sites·cm^{-2} on a heated glass plate. Pictures were taken with a high speed camera from underneath the plate.

* Corresponding author. Tel.: +49 (0)711 685 35 38; fax: +49 (0)711 685 3503.

E-mail addresses: hahne@itw.uni-stuttgart.de (E. Hahne), barthau@itw.uni-stuttgart.de (G. Barthau).

1290-0729/$ – see front matter
doi:10.1016/j.ijthermalsci.2004.10.009

Nomenclature

A	area on heated surface ..... cm^2	p^*	$= p/p_c$ reduced pressure
c'	specific heat capacity of saturated liquid ..... kJ·kg^{-1}·K^{-1}	q	heat flux ..... W·m^{-2}
D_B	bubble departure diameter ..... mm	r_c	critical radius ..... µm
h	heat transfer coefficient ..... W·m^{-2}·K^{-1}	s	average bubble spacing ..... mm
Δh_v	heat of evaporation ..... kJ·kg^{-1}	T_s	saturation temperature ..... K
Ja	$= (\rho' \cdot c' \cdot \Delta\vartheta)/(\rho'' \cdot \Delta h_v)$ Jakob-number	t	time ..... sec
N	number of active nucleation sites	$\Delta\vartheta$	$= \vartheta_{\text{wall}} - \vartheta_{\text{liquid}}$ excess temperature ..... K
N/A	nucleation site density ..... cm^{-2}	$\Delta\vartheta_{\text{loc}}$	$= \vartheta_{\text{wall,loc}} - \vartheta_{\text{liquid}}$ local excess temperature ... K
P	heat flow per nucleation site ..... mW	ρ'	liquid density ..... kg·m^{-3}
p	pressure ..... bar	ρ''	vapour density ..... kg·m^{-3}
Δp	pressure difference ..... Pa	σ	surface tension ..... N·m^{-1}

Iida and Kobayasi [26] applied a miniature void-detection probe to operate within a small distance above the heated surface. They encountered up to 150 sites·cm^{-2}.

Meyers and co-workers [27,28] worked with an electrically heated stainless steel sheet with a liquid crystal coating or used a high speed infrared camera, to identify the active sites on the upper surface.

Barthau [29] was able to count up to 8000 sites·cm^{-2}on the vertical flank of a horizontal tube, using an optical method.

Pinto [30] succeeded in measuring up to 40000 sites·cm^{-2}, also on the vertical flank of a horizontal tube with his high speed video camera.

For the investigation here, the optical method as presented in [29] was improved so that 14000 sites·cm^{-2} could be counted on the vertical flank of a horizontal copper tube [31].

2. Experimental set up and measuring method

Tests were performed on horizontal copper-tubes of 8 mm and 15 mm in diameter and on a stainless steel tube (15 mm). These tubes were either emery ground, sandblasted or gold plated. They had a length of 150 mm and 200 mm (8 mm diameter) and were heated electrically.

Our results have been compared with results from our partner (WKT, Institut für Energie- und Verfahrenstechnik, Universität Paderborn, Germany).

In Table 1 a list is given of the various test specifications.

Details and the measuring method are described in [29,31–33].

For the counts of the nuclei, the tube was viewed by a video camera through a telescope. Depending on the nucleation site density, different sizes of the observed areas, i.e. different magnifications (maximum 420 times), had to be selected. When the tube surface is observed in directly reflected light, the nucleation sites with their adhering bubbles appear as dark spots. These are marked on a transparent foil placed on the video screen.

3. Results for heat transfer coefficients

Heat transfer coefficients h were measured in a pressure range of 4.1 bar to 28.4 bar (i.e. $0.1 \leqslant p^* \leqslant 0.7$) for R134a and 1.5 bar to 2.47 bar ($0.05 \leqslant p^* \leqslant 0.074$) for R114. Results are shown in Fig. 1 for $p^* = 0.1, 0.5$, and 0.7. The gold-plated (sandblasted) tube gives the biggest heat transfer coefficients for a $p^* = 0.5$. These exceed the emery ground tube (15 mm diameter) by 20 to 30%. For $p^* = 0.1$ there is only little difference between the gold-plated tube and the emery ground one, therefore this cannot be distinguished in Fig. 1.

The stainless steel tube renders the smallest heat transfer coefficients. Compared to gold-plated-tube data for small heat fluxes, the heat transfer coefficients for the sandblasted stainless steel tube are below by about 30%, for high heat fluxes by 15%.

The heat transfer coefficients for the 8 mm tube and R114 are about 20% below those of the emery ground 15 mm tube in R134a.

For the stainless steel tube a special arrangement of thermocouples had to be made in order to obtain reliable thermal conductivity data for the steel material. Inside the tube, on top and bottom and either side, 2 thermocouples were positioned at different radii 0.9 mm and 2.8 mm below the heating surface.

Table 1
Test specifications

Place	Material	d [mm]	Surface finish	R_a [µm]	Fluid	Reference
Stuttgart	Copper	8	emery ground	0.52	R114	29
Stuttgart	Copper	15	emery ground	0.40	R134a	31
Stuttgart	Copper, gold-plated	15	sandblasted	0.30	R134a	32
Stuttgart	Stainless Steel	15	sandblasted	0.18	R134a	33
Paderborn	Copper–Nickel	24	sandblasted	0.21	R134a	priv.com.
Paderborn	Copper	25.4	sandblasted	0.25	R134a	priv.com.

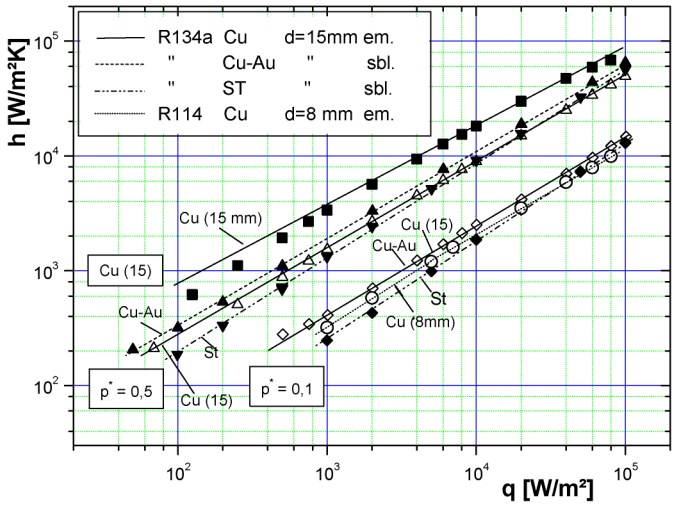

Fig. 1. Heat transfer coefficient h vs. heat flux q for different configurations and pressures. em—emery ground; sbl—sandblasted.

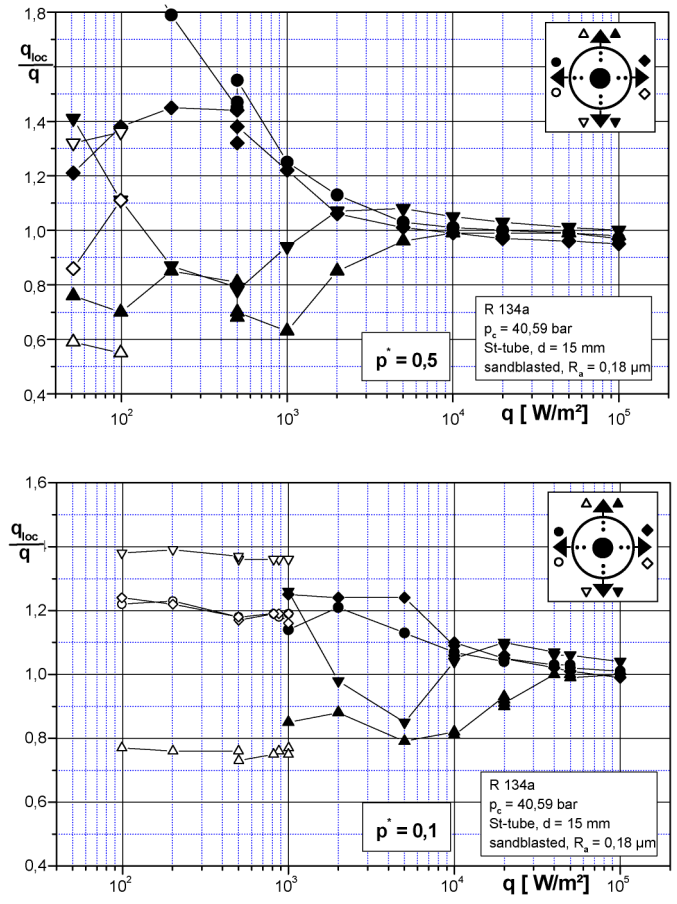

Fig. 2. Ratio of the local heat flux q_{loc} to the average heat flux q vs. heat flux q for two reduced pressures p^*. Open symbols: single phase natural convection.

This arrangement also allowed for the measurement of local heat fluxes and local heat transfer coefficients. The results of these circumferential distributions are shown in Figs. 2 and 3.

In Fig. 2 the ratio of the local heat flux q_{loc} to the average heat flux q (obtained from the electrical input) is plotted vs. the average heat flux. Due to symmetry the local heat fluxes

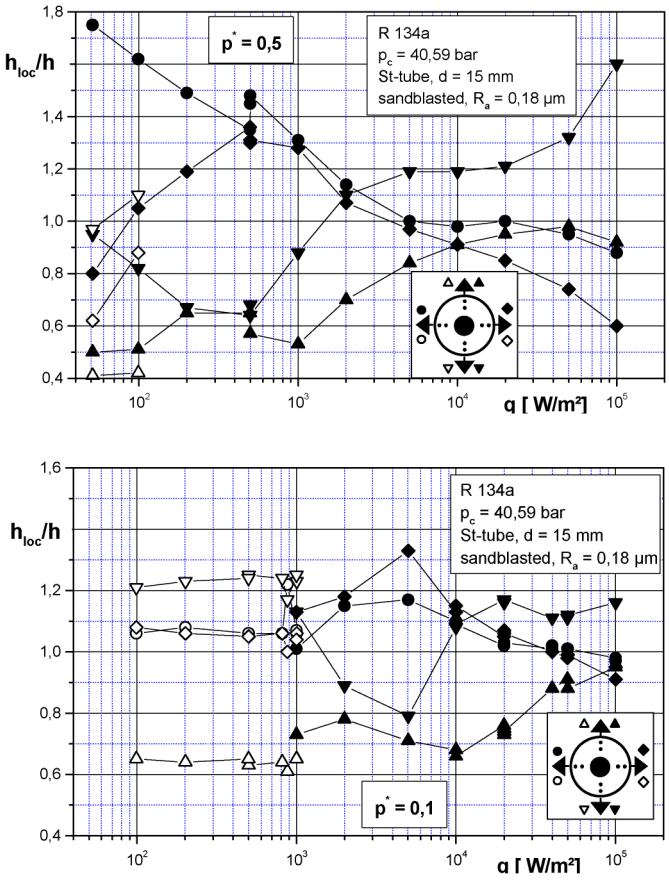

Fig. 3. Ratio of the local heat transfer coefficient h_{loc} to the average heat transfer h vs. heat flux q for two reduced pressures p^*. Open symbols: single phase natural convection.

on either side should be the same. The deviations in the low heat flux range ($q \leqslant 10^3$ W·m^{-2}) are thought to be caused rather by different nucleation site distributions than by measurement errors. This can be deduced from the behaviour of the corresponding data for natural convection (open symbols), which show nearly perfect agreement. At highest heat fluxes, $q \approx 10^5$ W·m^{-2}, all local deviations nearly disappear. The accuracy of these data is given mainly by the accuracy of the position of the individual thermocouple junctions and is estimated to be ±5%.

The ratio of the local heat transfer coefficient $h_{\mathrm{loc}} = q_{\mathrm{loc}}/\Delta\vartheta_{\mathrm{loc}}$ to the average heat transfer coefficient $h = q/(\Delta\vartheta)_{\mathrm{av}}$ is plotted vs. the heat flux in Fig. 3 for the pressure ratios $p^* = 0.1$ and 0.5. For $p^* = 0.1$ it can be seen that the local heat transfer coefficient for single phase natural convection is independent of heat flux. The same is true for $p^* = 0.3$; 0.15 and 0.03 which is not shown here. The heat transfer coefficient is highest at the bottom and lowest at the top of the tube.

In the boiling region h_{loc} is highest at the bottom for all pressures and heat fluxes $q > 10^4$ W·m^{-2}.

In this joint program we were able to compare our measurement data of the emery ground 15 mm Cu-tube to those from Paderborn with a sandblasted 24 mm CuNi-tube and 25.4 mm Cu-tube. Amazingly the results of either laboratory agree more or less with each other despite of differences in tube-material,

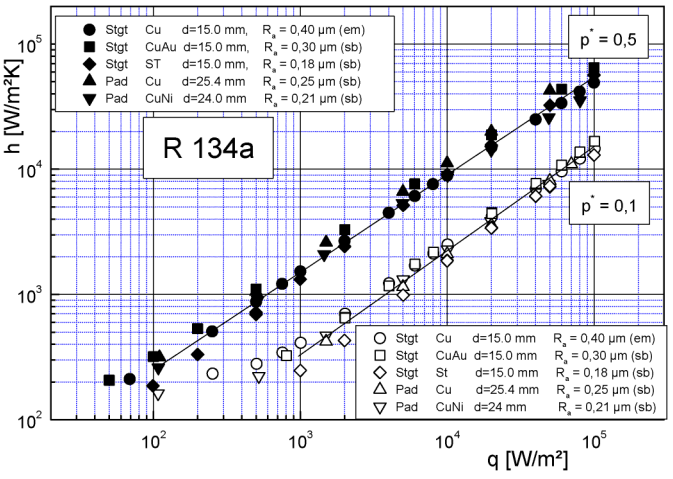

Fig. 4. Comparison of heat transfer results on different tubes with different surface finish.

-diameter and surface finish with different roughness parameters, Fig. 4.

4. Results for nucleation

Of the many potential bubble sites on a heated surface only those are counted here which produce bubbles—continuously or intermittently, i.e. are active, permanently or with inactive intermissions. Long term and short term observation have shown that quite different results are obtained for the nucleation site density in either case. There are various names given in literature to this phenomenon: here we want to clearly specify the conditions which have led to the observations: long term nucleation site densities are observed for the length of some 10 minutes, short term nucleation site densities for fractions of seconds.

This does not mean, however, that the long term sites must be active over the entire period of observation; often they are not.

Judd and Merte [34] were, as far as we know, the first to distinguish between an "average population density" i.e. the number of bubbles per unit area at a given instant (short term), and "active site density" i.e. the total number of active sites per unit area (long term). To make it more evident we prefer to speak of short- and long-term events. Judd and Merte found that the short-term population density is approximately one half of the long-term population density for the same levels of heat flux. The same observation was made by Barthau [29].

5. Long term nucleation

Here observations were performed for 15 to 30 minutes. In Fig. 5 long term nucleation site densities are shown vs. heat flux. On the right-hand side of the diagram the visualised areas A_{vis} are indicated. For high population densities only small areas (0.5 to 1 mm^2) could be chosen.

In this diagram long term site densities are shown, for three different pressures $p^* = 0.1$; 0.5; 0.7 and for the different test tubes listed in the insert.

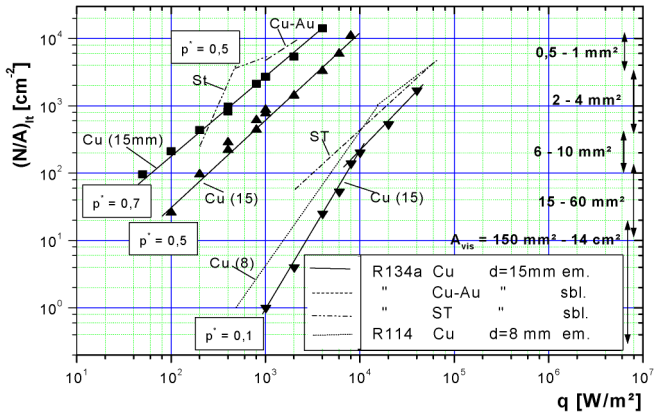

Fig. 5. Long term nucleation site density $(N/A)_{\text{lt}}$ vs. heat flux q for different tubes with different surface finish.

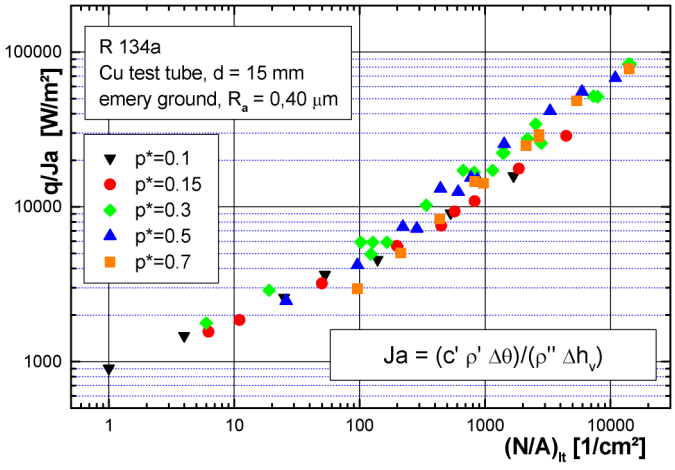

Fig. 6. Relation between heat flux divided by the Jakob-number q/Ja and long term nucleation site density $(N/A)_{\text{lt}}$.

The site density increases with heat flux and pressure. The increase of site density with heat flux $(\Delta(N/A)/\Delta q)_p$ is larger than 1. It is interesting to notice that N/A can increase by almost 1000 times when the pressure is increased only 5 times, e.g. from $p^* = 0.1$ to $p^* = 0.5$.

For $p^* = 0.5$ the sandblasted tubes exhibit a higher density than the emery ground tube and even the emery ground tube for $p^* = 0.7$.

In these studies it was observed that the sites are permanently active only at very low heat fluxes, i.e. at low nucleation site densities. They become intermittently active when the heat flux is increased.

In an attempt to correlate these different curves we plotted the heat flux divided by the Jakob-number vs. the long term nucleation site density, Fig. 6. The Jakob-number, which characterizes the ratio of the sensible heat to the latent heat of a given fluid volume is often used to describe bubble dynamics. The various curves do come together, but a satisfactory correlation is best only at small $N/A < 100$ cm^{-2} .

The interrelation of the nucleation site density with the averaged heat transfer coefficient h is shown in Fig. 7. Results for the emery ground Cu-tube and the sandblasted Cu–Au and stainless steel tubes are compared. It seems logic that the heat

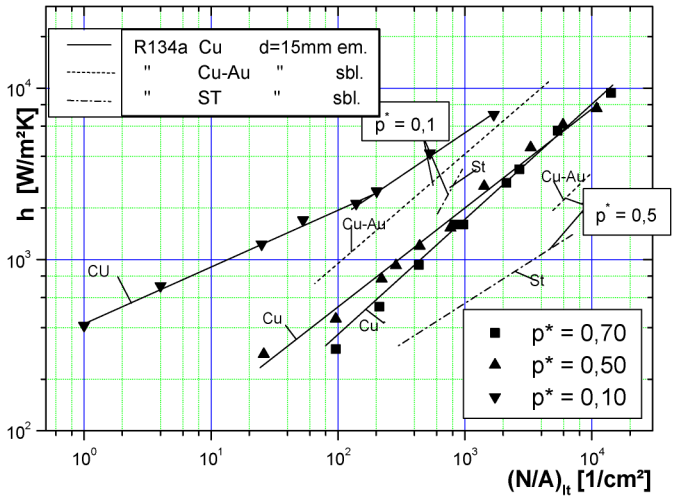

Fig. 7. Heat transfer coefficient h vs. long term nucleation site density $(N/A)_{\mathrm{lt}}$ for different tubes.

transfer coefficient increases, when the site density increases. But not in all cases the increase in N/A is accompanied by an equivalent increase in h: e.g. $\Delta(N/A)$ can be larger or smaller than Δh.

For the same pressure, the same number of sites brings forth the highest heat transfer coefficient on an emery ground Cu-tube, followed by the sandblasted Cu–Au-tube and the stainless steel tube.

For the same nucleation site density an increase in pressure causes a decrease for the heat transfer coefficient. This might be due to smaller bubbles at higher pressures.

The performance of a nucleus depends on its critical radius. This is a property defined by

$$r_c = 2 \cdot \sigma / \Delta p = (2 \cdot \sigma \cdot T_s)/(\Delta h_v \cdot \rho'' \cdot \Delta\vartheta) \tag{1}$$

with σ surface tension, T_s saturation temperature, Δh_v heat of evaporation, ρ'' vapour density and $\Delta\vartheta = \vartheta_{\mathrm{wall}} - \vartheta_{\mathrm{liquid}}$ the excess temperature.

In Fig. 8 a plot is presented of a cumulative number of active nucleation sites vs. the critical radius. This $(N/A)_{\mathrm{cum}}$ has to be introduced since—different from the common use of diagrams, the number here does not result from *one* r_c e.g. $(N/A)_{\mathrm{cum}} = 10^2$ cm^{-2} for $r_c \approx 0.4$ μm, but it is the accumulated number of active sites with critical radii $\geqslant r_c$. The large nucleation sites become active already at small $\Delta\vartheta$ (or q), more and more sites become active as the wall temperature increases until the respective r_c for the condition given in Eq. (1) is reached, e.g. $r_c \approx 0.4$ μm in the aforementioned example.

It is well known that more and more sites become active when the heat flux, i.e. the excess temperature is increased, which causes the critical radius to decrease. This is verified in Fig. 8.

Data for different tubes and fluids are presented in this figure: pressure ratios of $p^* = 0.1$–0.7 were obtained on an emery ground Cu-tube, 15 mm diameter in R134a, the dashed line indicates data from Luke et al. [35] for a sandblasted 25.4 mm Cu-tube in propane. The curve on the right boundary represents

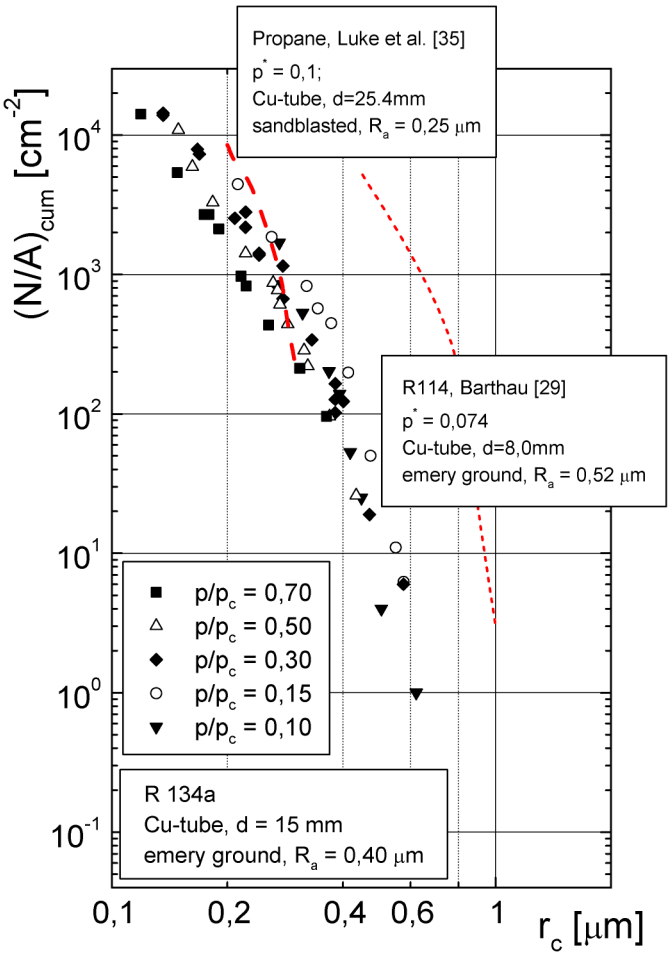

Fig. 8. Cumulative nucleation site density $(N/A)_{\mathrm{cum}}$ vs. critical radius r_c for different reduced pressures.

data for an emery ground 8 mm Cu-tube in R114 [29]. These latter were obtained for $p^* \approx 0.1$.

6. Short term nucleation

These observations were performed with a camera; our results are based on an exposure time of 1/60 sec.

In Fig. 9 the ratio of short term to long term nucleation site density is presented vs. heat flux. This result is obtained on the emery ground 15 mm Cu-tube [31].

It shows that the number of sites counted in short term observations is almost always smaller than that for long term observations. In some cases only about half.

This is even more pronounced for the sandblasted Cu–Au-tube [32], as is shown in Fig. 10. Again, the short term data are smaller than the long term data, but when the ratio $(N/A)_{\mathrm{st}}/(N/A)_{\mathrm{lt}}$ is considered, we may obtain ratios of an order of magnitude smaller than in Fig. 9, e.g. for $p^* = 0.5$ at $q = 2000$ W·m^{-2}. In any case $(N/A)_{\mathrm{st}}/(N/A)_{\mathrm{lt}}$ is now below 0.5 while in Fig. 9 it used to be in the range of 0.5 to 1.0.

A big difference is obvious when the bubble production on the surface is directly observed: On emery ground surfaces the nucleation appears in the longitudinal direction of grinding. In grooves along the tube bubbles appear like pearls on a string. At

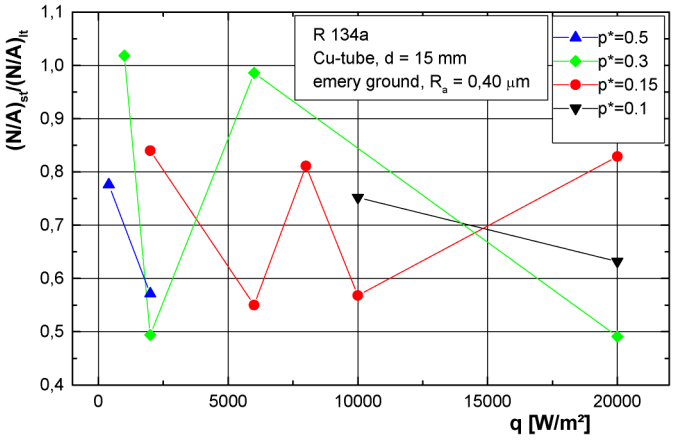

Fig. 9. Ratio of short term to long term nucleation site density depending on heat flux.

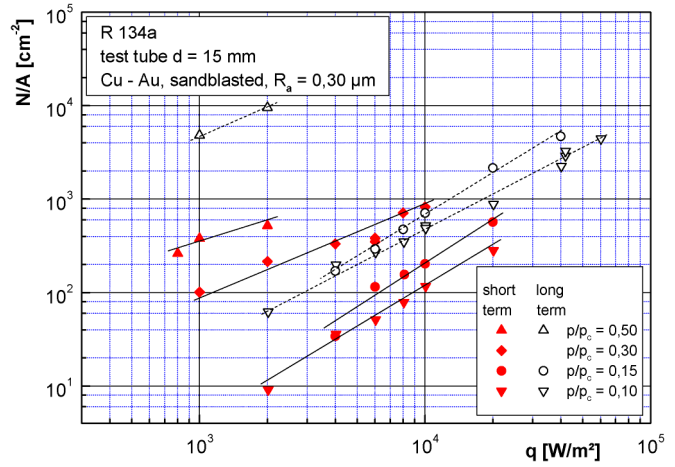

Fig. 10. Long term and short term nucleation site density depending on heat flux.

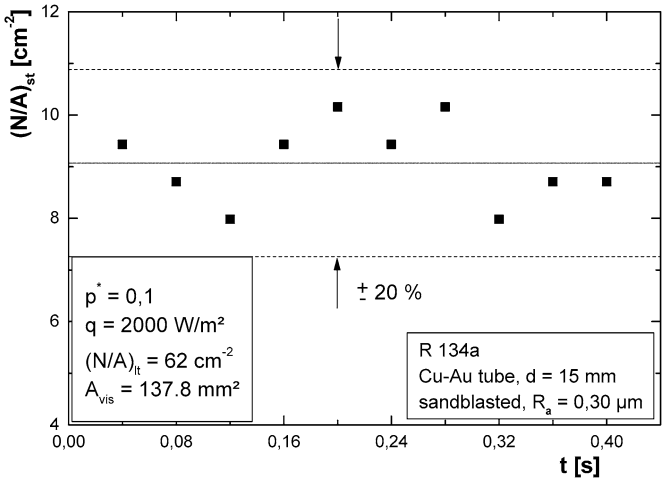

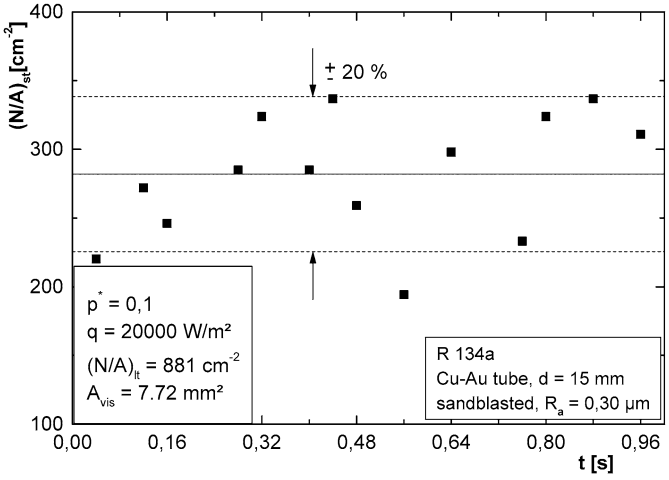

Fig. 11. Short term nucleation site density vs. time of consecutive exposures for two heat fluxes.

small fluxes these sites appear very stably: they produce bubbles for hours continuously. At high heat fluxes such stable sites are scarce. Sites come and go and produce bubbles irregularly.

For our sandblasted tubes a very uniform surface—feeling sort of rough—had been obtained. It seems that on this tube more equally sized sites exist than on the emery ground tubes. The sites here, however, appear short-lived and jumping from one place to another; permanently new sites appear in new places. In this case it seems impossible to find a correlation between the bubbles and the sites as one could have the impression that the active sites migrate to the heat and not the heat to the site as is assumed for the stable sites. On emery ground surfaces the stability of active sites, i.e. a continuous bubble production, seems to last longer than on sandblasted surfaces.

The temporal changes in nucleation site density are shown in Fig. 11 for the sandblasted gold covered Cu tubes. The results are presented for two different heat fluxes. The frames were obtained from a film projected on a TV-screen and analysed frame by frame. The exposure time was 1/60 sec. It can be seen, that the number of active sites changes around 9 $\mathrm{cm}^{-2} \pm 20\%$ for $q = 2000\ \mathrm{W{\cdot}m^{-2}}$; for 20 000 $\mathrm{W{\cdot}m^{-2}}$ it is around 280 $\mathrm{cm}^{-2} \pm 20\%$.

For comparison, the number of sites obtained in long term observation is 60 cm^{-2} for an observed area of 137.8 mm^2 and 880 cm^{-2} for 7.72 mm^2.

From these observations the lower values of short term sites compared to long term sites might find an explanation in the above mentioned intermittent activity of nucleation sites: In short term observation fewer sites may become apparent than in long term observations, due to the high instability of sites in combination with a much smaller exposure time.

7. Heat flow from individual sites

From the experiments with the emery ground tube [31] the heat flow delivered by one single nucleation site was evaluated. The results for various pressures are presented in Fig. 12. The individual heat flow per nucleus is largest for the smallest pressure. This, of course can be deduced clearly from Fig. 5: the same heat flux, e.g. $q = 10^3\ \mathrm{W{\cdot}m^{-2}}$, requires for $p^* = 0.7$ a number of nucleation sites which is more than 3 orders of magnitude larger than for $p^* = 0.1$. Consequently, in Fig. 12 the heat flow for $p^* = 0.7$ is smaller by more than 3 orders of magnitude. The heat flow decreases for increasing heat fluxes.

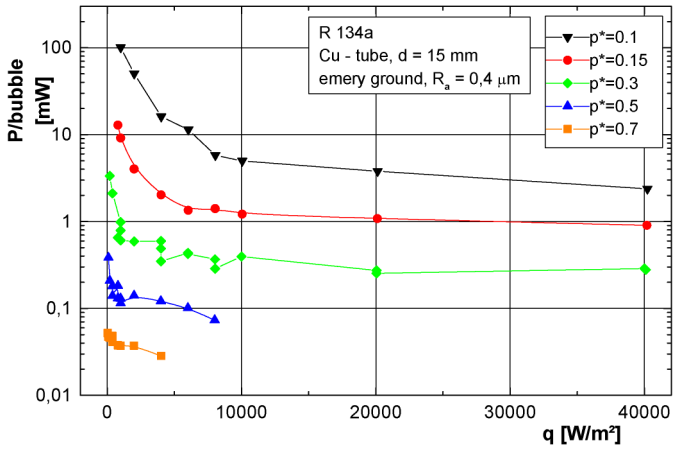

Fig. 12. Heat flow P per nucleation site depending on heat flux.

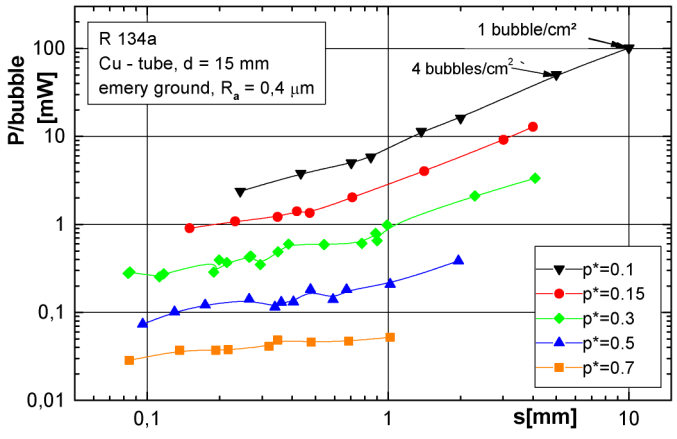

Fig. 13. Heat flow P per nucleation site depending on average bubble spacing s; $s = 1/(N/A)^{0.5}$.

Zuber [36] proposed a theoretical distance between bubbles; this he called "average bubble spacing" and defined it as

$$s = (N/A)^{-0.5} \tag{2}$$

bubbles would touch each other when $s = D_B$, i.e. when the bubble distance reaches the bubble departure diameter.

A plot, heat flow P per nucleation site vs. average bubble spacing s, is given in Fig. 13. This shows that few bubbles with consequently large spacing give a large heat flow per bubble and its pro-rata surrounding surface. But more bubbles, with small spacing, altogether release more heat. For $p^* = 0.1$, e.g., 1 bubble·cm^{-2} with a spacing of 10 mm gives 100 mW while 4 bubbles·cm^{-2} with a spacing of 5 mm give 50 mW each, altogether 200 mW. If we try to bring the various curves together the Jakob-number Ja again appears helpful.

A plot of P/Ja vs. s is shown in Fig. 14. For the lower pressure range $p^* \leqslant 0.3$ and a small number of nucleation sites the fit seems satisfactory, but for $s \leqslant 1$ mm, i.e. 100 sites·cm^{-2} or more, deviations of ±50% can be observed.

A plot of q/Ja vs. s as shown in Fig. 15, indicates the same behaviour as Fig. 14: satisfactory agreement for small numbers of nucleation sites but too big deviations for large numbers.

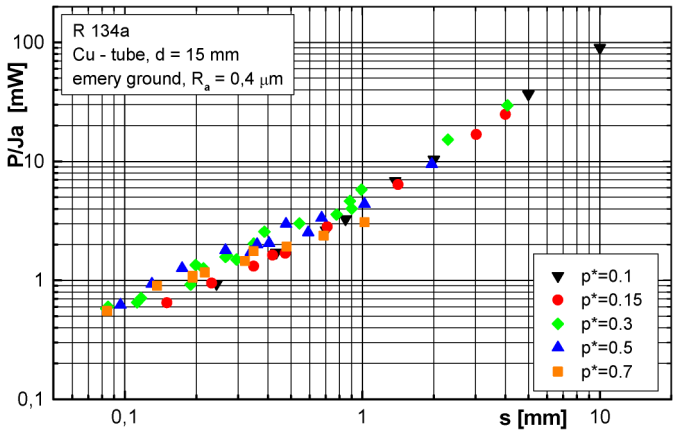

Fig. 14. Heat flow per nucleation site divided by Jakob-number vs. average bubble spacing, based on long term observation.

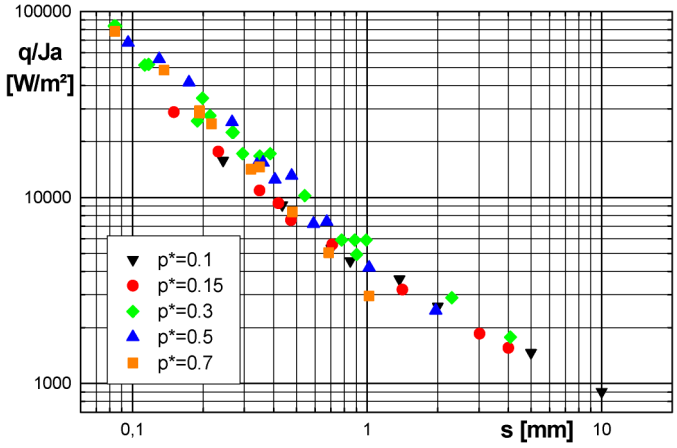

Fig. 15. Heat flux divided by Jakob-number vs. average bubble spacing, based on long term observation.

8. Conclusions

Roughly speaking there is not too much difference in the heat transfer coefficients of

- Cu-, Cu–Ni-, Cu gold-plated-, or stainless steel tubes;
- Emery ground or sandblasted;
- 8, 15, 24 or 25.4 mm diameter;
- R_a measured from 0.18 to 0.40 µm;
- Measured at Paderborn or Stuttgart.

The scatter is within 30%.

Looking more closely, however, there are of course differences within this uncertainty range:

Gold-plated and sandblasted Cu-tubes have higher heat transfer coefficients than emery ground (unplated) tubes for $p^* = 0.5$, not so however for $p^* = 0.1$.

In any case the stainless steel tube has lower heat transfer coefficients for $q \leqslant 30\,000$ W·m^{-2} than any of the other tubes.

For materials with low thermal conductivity (e.g. stainless steel) one has to be aware that local heat fluxes around a horizontal tube are far from being uniform. Deviations in heat flux

and heat transfer coefficients between bottom and top or side and top may amount to 100%.

In the determination of nucleation site densities the differences in long term and short term observations have to be considered. This difference for emery ground tubes can come up to a factor of two, for sandblasted tubes, however, to almost two orders of magnitude.

So far a correlation between heat flux, respectively heat transfer and nucleation site density seems yet quite uncertain or applicable only to few data.

Acknowledgement

The authors highly appreciate the financial support by the Deutsche Forschungsgemeinschaft (DFG) for the investigations performed within the German research program “Thermo- and Fluiddynamics in Boiling”. We also want to thank Prof. Dr. D. Gorenflo, for the valuable cooperation and Dr.-Ing. Habil. Andrea Luke for preparing the test-tubes’ surfaces and measuring their surface structure.

The high purity R134a was supplied by Solvay Company. We gratefully acknowledge this support.

References

[1] M. Jakob, W. Fritz, Versuche über den Verdampfungsvorgang, Forsch. Ing. Wes. 2 (1931) 435–447.
[2] M. Jakob, W. Linke, Der Wärmeübergang von einer waagrechten Platte an siedendes Wasser, Forsch. Ing. Wes. 4 (1933) 75–81.
[3] C. Corty, Surface variables in boiling, PhD thesis, University of Michigan, 1951.
[4] C. Corty, A.S. Foust, Surface variables in nucleate boiling, Chem. Engrg. Prog. Sympos. Ser. 17 (1955) 51.
[5] S.G. Bankoff, Proc. Heat Transfer Fluid Mechanics Inst, Stanford University Press, Stanford, CA, 1956.
[6] K. Nishikawa, Studies on heat transfer in nucleate boiling, Mem. Fac. Engrg. Kyushu Univ. 16 (1956) 1–28.
[7] J.W. Westwater, P.H. Strenge, Active sites and bubble growth during nucleate boiling, Chem. Engrg. Prog. Sympos. Ser. 29 (1959) 95 and 16 mm movie, Engineering Societies Library, New York, 1958.
[8] P. Griffith, D.W. Wallis, The role of surface conditions in nucleate boiling, Chem. Engrg. Prog. Sympos. Ser. 56 (30) (1960) 49–63.
[9] H.M. Kurihara, J.E. Myers, The effect of superheat and surface roughness on boiling coefficient, AIChE J. 6 (1960) 83–91.
[10] C.Y. Han, P. Griffith, The mechanism of heat transfer in nucleate pool boiling, Int. J. Heat Mass Transfer 8 (1965) 887–914.
[11] P. Griffith, Nucleation and bubble formation in boiling, Sympos. Boiling Heat Transfer, Proc. Inst. Mech. Engrg. 180 (1956–1966), Pts. 1 and 3C.
[12] W.M. Rohsenow, Nucleation with boiling heat transfer, Ind. Engrg. Chem. 58 (1966) 1.
[13] A.P.Hatton, I.S. Hall, Photographic study of boiling on prepared surfaces, in: Proc. 3rd Int. Heat Transfer Conf., Chicago, vol. 4, 1966, pp. 24–37.
[14] M. Güttinger, Die Verbesserung des Wärmeübergangs bei der Verdampfung in überfluteten Rohrbündelverdampfern, in: Proc. 4th Int. Heat Transfer Conf., Paris-Versailles, vol. 1, 1970, Paper HE 2.4.
[15] H.M. Kottowski, Nucleation and superheating effects on activation energy of nucleation, Progr. Heat Mass Transfer 7 (1973) 299–324.
[16] R. Cole, Boiling nucleation, Adv. Heat Transfer 10 (1974) 86–164.
[17] J.J. Lorenz, B.B. Mikic, W.M. Rohsenow, Effects of surface conditions on boiling characteristics, in: Proc. 5th Int. Heat Transfer Conf., Tokyo, 1974, vol. 4, 35, Paper B2.1.
[18] A. Singh, B.B. Mikic, M. Rohsenow, Active sites in boiling, J. Heat Transfer 98 (1976) 401–406.
[19] R.I. Eddington, D.B.R. Kenning, The prediction of flow boiling bubble population from gas bubble nucleation experiments, in: Proc. 6th Int. Heat Transfer Conf., Toronto, 1978, vol. 1, pp. 275–279.
[20] K. Cornwell, R.D. Brown, Boiling surface topography, in: Proc. 6th Int. Heat Transfer Conf., Toronto, vol. 1, 1978, pp. 157–161.
[21] S. Faggiani, P. Galbiati, W. Grassi, Active site density, bubble frequency and departure diameter in water and Freon 113 boiling on chemically etched surfaces, La Termotecnica 35 (1981) 511–519.
[22] M. Siebert, Untersuchung zum Einfluß des Wandmaterials und des Rohrdurchmessers auf den Wärmeübergang von horizontalen Rohren an siedende Flüssigkeiten, Diss. Univ. Karlsruhe, Germany, 1987.
[23] R.F. Gaertner, J.W. Westwater, Population of active sites in nucleate boiling heat transfer, Chem. Engrg. Prog. Sympos. Ser. 56 (30) (1960) 39–48.
[24] R.L. Semeria, An experimental study of the characteristics of vapour bubbles, in: Symp. Two-phase Fluid Flow, London, 1962, Paper 7.
[25] D.B. Kirby, J.W. Westwater, Bubble and vapor behavior on a heated horizontal plate during pool boiling near burnout, Chem. Engrg. Prog. Sympos. Ser. 61 (57) (1965) 238–248.
[26] Y. Iida, K. Kobayasi, An experimental investigation on the mechanism of pool boiling phenomena by a probe method, in: Proc. 4th Int. Heat Transfer Conf., Paris-Versailles, vol. 5, 1970, Paper B1.3.
[27] T. Raad, J.E. Myers, Nucleation studies in pool boiling on thin plates using liquid crystals, AIChE J. 17 (1971) 1260–1261.
[28] J.E. Sgheiza, J.E. Myers, Behavior of nucleation sites in pool boiling, AIChE J. 31 (1985) 1605–1613.
[29] G. Barthau, Active nucleation site density and pool boiling heat transfer—an experimental study, Int. J. Heat Mass Transfer 35 (1992) 271–278.
[30] A.D. Pinto, Wärmeübergang und Blasenbildung beim Sieden von Propan an einem geschmirgelten Kupferrohr in einem großen Druckbereich, Diss. Univ. Paderborn, Germany, 1995.
[31] G. Barthau, E. Hahne Nucleation site density and heat transfer in nucleate pool boiling of refrigerant R134a in a wide pressure range, in: Proc. 3rd European Thermal-Sciences Conf., Heidelberg, 2000, vol. 2, pp. 731–736.
[32] G. Barthau, E. Hahne, Nucleate pool boiling of refrigerant R134a on a gold-plated copper test tube, in: Conf. Int. Inst. Refrigeration, Commission B1, Paderborn, Germany, 2001.
[33] G. Barthau, E. Hahne, Experimental study of nucleate pool boiling of R134a on a stainless-steel tube, Int. J. Heat Fluid Flow 25 (2004) 305–312.
[34] R.L. Judd, H. Merte, Influence of acceleration on sub-cooled nucleate pool boiling, in: Proc. 4th Int. Heat Transfer Conf., Paris-Versailles, vol. 6, 1970, Paper B8.7.
[35] A. Luke, E. Danger, D. Gorenflo, Size distribution of active and potential nucleation sites in pool boiling, in: Proc. 12th Int. Heat Transfer Conf. Grenoble, France, vol. 3, 2002, p. 383.
[36] N. Zuber, The region of isolated bubbles and the similarity with natural convection, Int. J. Heat Mass Transfer 6 (1963) 53–78 (originally in an AEC Report in January 1960).